



Article

Understanding the Leakage Mechanisms and Breakdown Limits of Vertical GaN-on-Si p^+n^-n Diodes: The Road to Reliable Vertical MOSFETs

Kalparupa Mukherjee ^{1,*}, Carlo De Santi ¹, Matteo Buffolo ¹, Matteo Borga ², Shuzhen You ², Karen Geens ², Benoit Bakeroot ³, Stefaan Decoutere ², Andrea Gerosa ¹, Gaudenzio Meneghesso ¹, Enrico Zanoni ¹ and Matteo Meneghini ¹

¹ Department of Information Engineering, University of Padua, 35131 Padova, Italy; desantic@dei.unipd.it (C.D.S.); matteo.buffolo@dei.unipd.it (M.B.); gerosa@dei.unipd.it (A.G.); gauss@dei.unipd.it (G.M.); zanoni@dei.unipd.it (E.Z.); menego@dei.unipd.it (M.M.)

² Imec, Kapeldreef 75, 3001 Leuven, Belgium; matteo.borga@imec.be (M.B.); shuzhen.you@imec.be (S.Y.); karen.geens@imec.be (K.G.); stefaan.decoutere@imec.be (S.D.)

³ CMST IMEC/UGent, 9052 Ghent, Belgium; benoit.bakeroot@imec.be

* Correspondence: mukherjee@dei.unipd.it

Abstract: This work investigates p^+n^-n GaN-on-Si vertical structures, through dedicated measurements and TCAD simulations, with the ultimate goal of identifying possible strategies for leakage and breakdown optimization. First, the dominant leakage processes were identified through temperature-dependent current–voltage characterization. Second, the breakdown voltage of the diodes was modelled through TCAD simulations based on the incomplete ionization of Mg in the p^+ GaN layer. Finally, the developed simulation model was utilized to estimate the impact of varying the p-doping concentration on the design of breakdown voltage; while high p-doped structures are limited by the critical electric field at the interface, low p-doping designs need to contend with possible depletion of the entire p-GaN region and the consequent punch-through. A trade-off on the value of p-doping therefore exists to optimize the breakdown.

Keywords: semi-vertical; vertical; GaN; pn diodes; leakage modeling; device modeling; TCAD



Citation: Mukherjee, K.; De Santi, C.; Buffolo, M.; Borga, M.; You, S.; Geens, K.; Bakeroot, B.; Decoutere, S.; Gerosa, A.; Meneghesso, G.; et al. Understanding the Leakage Mechanisms and Breakdown Limits of Vertical GaN-on-Si p^+n^-n Diodes: The Road to Reliable Vertical MOSFETs. *Micromachines* **2021**, *12*, 445. <https://doi.org/10.3390/mi12040445>

Academic Editor: Giovanni Verzellesi

Received: 26 February 2021

Accepted: 13 April 2021

Published: 16 April 2021

Publisher's Note: MDPI stays neutral with regard to jurisdictional claims in published maps and institutional affiliations.



Copyright: © 2021 by the authors. Licensee MDPI, Basel, Switzerland. This article is an open access article distributed under the terms and conditions of the Creative Commons Attribution (CC BY) license (<https://creativecommons.org/licenses/by/4.0/>).

1. Introduction

Wide bandgap semiconductors (WBGs) are being widely advocated to meet the demands for higher efficiency, robustness, and power handling capabilities [1–16], as Si is approaching its limits in market sectors where high efficiency and high power are required, such as transportation, aerospace, and power conversion systems. The contenders include SiC [13,14], GaN, β -Ga₂O₃ [15], diamond [11,12], and AlN [16] in order of increasing bandgap and thus breakdown field. So far, only GaN and SiC have progressed from research-level devices to commercially available technologies, whereas β -Ga₂O₃, diamond, and AlN prototypes, while highly promising, have not yet reached the maturity for high level production.

Currently, SiC-based devices are dominating the WBG market for power applications requiring >1200 V, voltages that are not yet reached by commercial lateral GaN devices. However, GaN is superior to SiC in overall material properties (breakdown field, mobility, saturation velocity), making it the stronger choice for most applications. To further enhance the performance of GaN transistors, the focus of research is shifting from lateral to vertical architectures, which circumvent the breakdown limitations, surface trapping, and other challenges inherent to the lateral topology.

The adoption of GaN-based vertical diodes and transistors [1–7] is highly advantageous to high-speed and high-power electronics applications, presenting low R_{on} and higher breakdown robustness in addition to improved thermal performance. Preliminary

demonstrators of quasi-vertical or vertical diode structures [1–10] have already presented good performance metrics, handling the associated epitaxial challenges in various ways.

Within the GaN power field, emerging GaN-on-Si vertical technologies have the competitive advantage. However, owing to the lattice mismatch between GaN and Si, the epitaxial thicknesses and doping of the vertical stack require careful optimization to achieve high breakdown voltages. For well-designed structures, the drift region becomes especially relevant because it dominantly controls the reverse breakdown capability. Currently, the wide use of GaN-on-Si vertical devices is being impeded by the lack of understanding of the leakage mechanisms and breakdown of the vertical stack. Leakage paths along the passivation, drift, and other transition layers, and through the Si substrate can critically affect the reliability of GaN-on-Si diodes. Reverse leakage conduction can arise from electrode limited, surface limited, or bulk limited conduction mechanisms [5,7,17].

Hence, the study and identification of vertical leakage conduction and doping constraints to optimize breakdown voltage are major research concerns in the design of vertical pn GaN diodes and FETs [5–7]. This analysis is different from studies of leakage in lateral GaN devices. In lateral GaN transistors, the buffer is typically isolating and compensated with carbon; in vertical GaN devices, most of the stack is constituted by a drift region that is not intentionally doped and which needs to be highly conductive. To investigate the leakage and breakdown, technology computer aided design (TCAD) simulations provide cost-effective and versatile perspectives towards the optimization and design of these devices. In this work, we use a combination of TCAD simulations and experimental measurements to understand how to overcome the breakdown and leakage limits of GaN-on-Si vertical devices, and to provide general design rules.

Within this work, Section 2 presents the structural details of the investigated quasi-vertical GaN-on-Si diodes. Section 3 is divided into two parts: Section 3.1 presents the modeling of the reverse leakage current of the tested devices, to identify the dominant mechanism for low and high voltage ranges, while Section 3.2 uses a simplified TCAD model to understand how the nature of breakdown changes as a function of the chosen doping level within the p^+ body. Section 4 reviews the main results and concludes the work.

2. Materials and Methods

The p^+n^- diode is the core of the epitaxy of semi-vertical/vertical trench-MOSFETs [8–10]; hence, understanding its breakdown limits is fundamental for the development of robust vertical GaN transistors. The samples in this study are test vehicles for investigation into the p^+n^-n GaN-on-Si semi-vertical diode configuration (Figure 1), enabling the dedicated characterization of diode properties and doping effects.

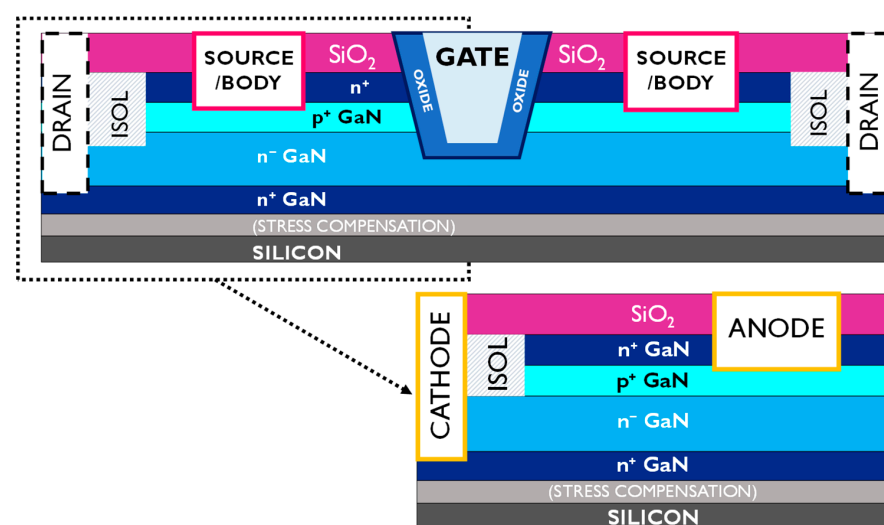


Figure 1. Schematic of the p^+n^- diode test vehicle structures, the fundamental unit of a complete semi-vertical MOSFET.

Fabricated on a 200 mm Si substrate, the diodes are based on an Mg-doped p^+ GaN body, where $N_A = 6 \times 10^{19} \text{ cm}^{-3}$, and a lightly doped n^- drift layer. The cathode is defined at the buried n^+ layer below the n^- drift region. The n^+ layers have a doping of $5 \times 10^{18} \text{ cm}^{-3}$, while the n^- drift layer has a doping of $N_D = 4 \times 10^{16} \text{ cm}^{-3}$. The parameters have been summarized in Table 1. For the p^+ GaN, the value of $N_A = 6 \times 10^{19} \text{ cm}^{-3}$ represents the test structures under test. However, the simulated p-doping levels have been varied to discuss the impacts of choosing low versus high p-doping values.

Table 1. Structural properties of the vertical GaN-on-Si diodes under test.

Layer (GaN)	Doping (cm^{-3})	Thickness (nm)
n^+	5×10^{18}	250
p^+ body	6×10^{19}	400
n^- drift	4×10^{16}	750

3. Results and Discussion

3.1. Physical Origin of Leakage Current

The conduction in the depletion region of a reverse biased p^+n^- junction can be considered analogous to leakage through a dielectric subjected to high fields [5,7,18]. The off-state leakage mechanisms can then be categorized with respect to (a) properties of the metal-dielectric (semiconductor) contact—referred to as electrode-limited conduction mechanisms, or (b) the properties of the dielectric, and thus the existing trap levels—referred to as bulk-limited conduction mechanisms. Both kinds of processes might be simultaneously applicable; however, electrode-limited mechanisms such as thermionic emission, Schottky emission, and direct or F–N tunneling should not be the limiting factors in well-designed vertical diodes with the peak field located deeper at the p^+n^- junction.

As such, the dominant mechanisms are usually bulk-limited, such as Poole–Frenkel emission, space charge limited conduction (SCLC), and variable range hopping (VRH), among others. To identify the vertical leakage mechanisms of the studied $p^+n^-n^-$ diodes, the temperature (T) dependence of the reverse biased diode characteristic is measured, as illustrated in Figure 2a.

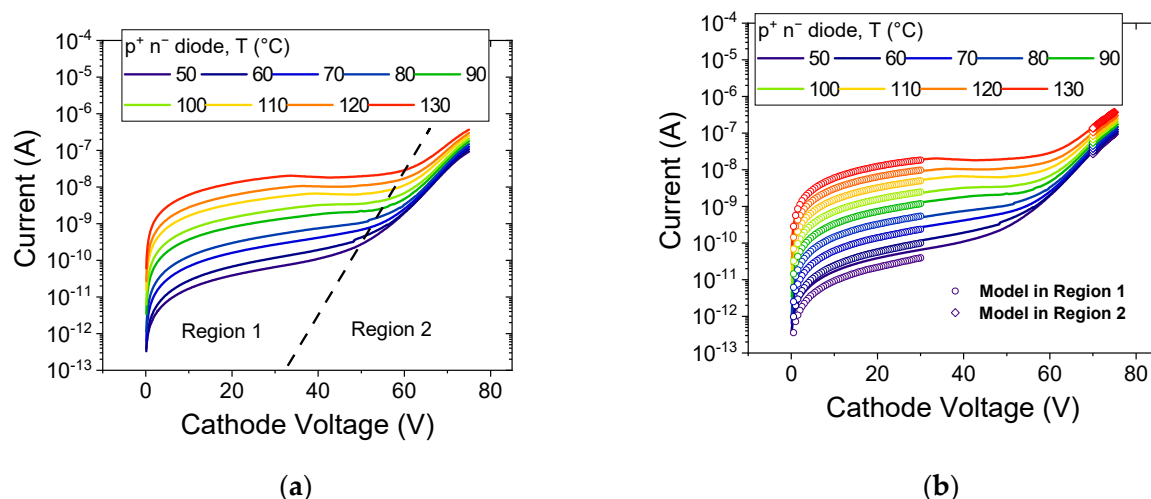


Figure 2. (a) Reverse leakage of the p^+n^- diodes measured for $T = 50 \text{ }^\circ\text{C}$ to $130 \text{ }^\circ\text{C}$. Two distinct regions can be identified; (b) illustrates the fit to the models used to describe the leakage evolutions in the two regions.

The curve exhibits two distinct regions (Region 1 and Region 2), with a notable second rise in slope for voltages higher than 40–60 V (depending on temperature). Each region has been modelled separately, as illustrated in Figure 2b, and described as follows.

The observed rapid rise in leakage with temperature implies a strong thermally activated process, which is modelled in Figure 3a using the following equation:

$$I_{TE} = AT^2 \exp\left(\frac{-E_A}{k_B T}\right), \tag{1}$$

This equation describes the temperature dependence of the current conduction originated by thermionic emissions from Coulombic traps [6,19]. Here, A is a constant defining the almost vertical shift of the curve, E_A is the thermal activation energy defining the slope of the curve, k_B is the Boltzmann constant, and T is the temperature. An activation energy of ≈ 0.85 eV is extracted from the slope in Figure 3b, indicating a possible role of carbon acceptors in the leakage process [20,21].

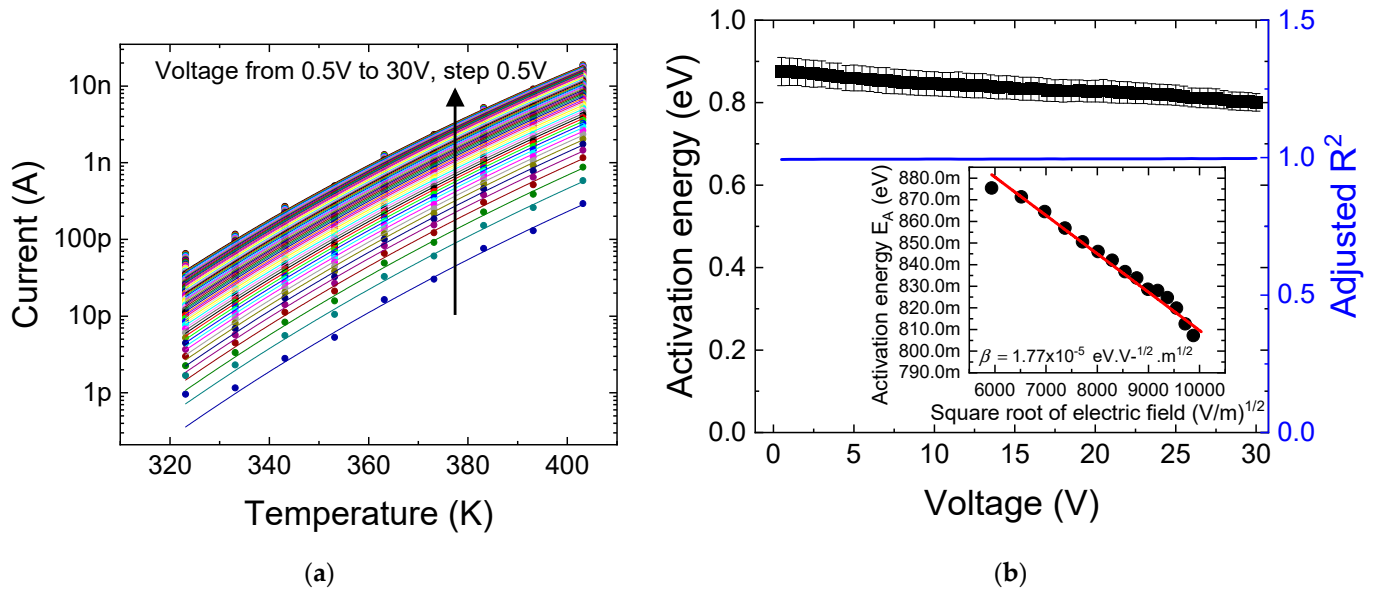


Figure 3. (a) Modeling reverse leakage diode behavior using Coulombic potential well model from 0 V to −30 V (Region 1) for $T = 50$ °C (323 K) to 130 °C (403 K); (b) extrapolated trap activation energy of 0.85 eV. The R^2 of the fit is near one in the entire analyzed voltage range, confirming the good quality of the fit. (inset) Lowering in E_A showing $F^{-1/2}$ dependence.

The corresponding conduction mechanism is described in Figure 4a. At low field F , the potential near traps can be assumed to be Coulombic, while at higher fields, the potential is deformed. Depending on the nature of the deformation, charge emission from an occupied primary trap state located at an energy of E_T from the conduction band minimum (CBM) (labelled A in Figure 4) can be strengthened through different conduction mechanisms. A higher temperature can lead to phonon assisted tunneling processes (contribution labelled PhaT in Figure 4a). With increasing temperature, the overall thermal energy of the trapped electron is higher, leading to a thinner barrier for carrier tunneling, as illustrated in the transition from A to B in blue in Figure 4a. However, under high fields, Poole–Frenkel lowering of the barrier height becomes relevant. A lower effective barrier can be directly overcome by the carriers by thermionic emission (contribution labelled PF in Figure 4a), as illustrated in the transition from A to B in red in Figure 4a. The Poole–Frenkel effect thus results in a change in the emission rate e_n [7,19,22,23] as follows:

$$e_n \propto \exp\left(-\frac{E_T - \beta F^{1/2}}{k_B T}\right). \tag{2}$$

This process facilitates emissions from trap centers at high fields (the Poole–Frenkel coefficient β quantifies the lowering in the barrier = $\beta\sqrt{F}$). As presented in the inset of Figure 4b, the field dependence of the extracted trap level at 0.85 eV is found to follow this behavior. The peak electric field values are taken from corresponding numerical simulations in the considered voltage range (described in detail in Section 3.2).

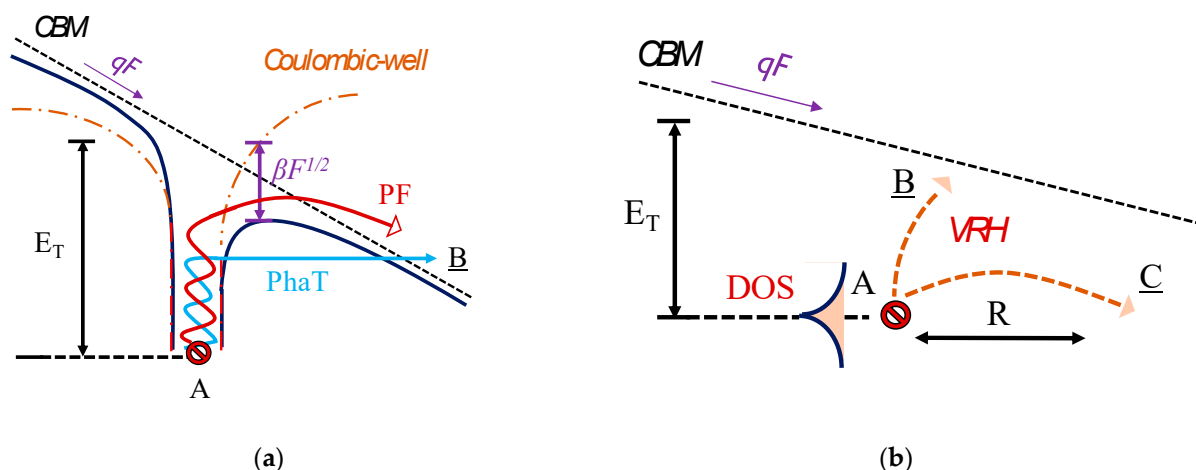


Figure 4. Schematic representation of the leakage processes: (a) Poole–Frenkel (PF) emission (used to model Region 1 in Figure 2); (b) variable range hopping (used to model Region 2 in Figure 2).

Theoretically, β can be written as $\beta = \sqrt{\frac{Zq^3}{\pi\epsilon}}$ [7,24,25], where Z represents the charge on the Coulomb center (ionization state of the trap), and ϵ is the permittivity of GaN. The extracted $\beta = 1.77 \times 10^{-5} \text{ eV V}^{-1/2} \text{ m}^{1/2}$ in our measurements is close to the theoretical value ($\approx 3.1 \times 10^{-5} \text{ eV V}^{-1/2} \text{ m}^{1/2}$) considering a relative high-frequency GaN permittivity of 5.8, and $Z = 1$ for the carbon acceptor. Considering a simplified $\beta = \sqrt{\frac{q}{\pi\epsilon}}$ [26], theoretical values are close to $3.2 \times 10^{-5} \text{ eV V}^{-1/2} \text{ m}^{1/2}$ [27–29]. Depending on the growth conditions in different GaN-based works, $\beta \approx 10^{-5} \text{ eV V}^{-1/2} \text{ m}^{1/2}$ are generally reported [7,24,25,27–34], as summarized in Figure 5.

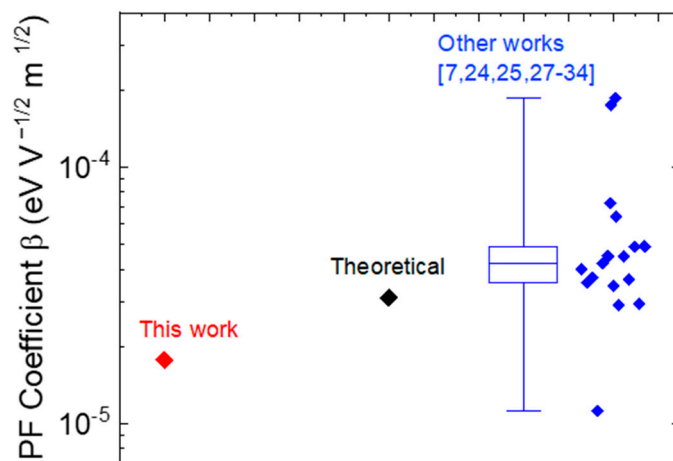


Figure 5. Comparison of the Poole–Frenkel coefficient ($\beta \approx 10^{-5} \text{ eV V}^{-1/2} \text{ m}^{1/2}$) obtained from different works on GaN-based systems [7,24,25,27–34].

For the second region of the leakage curves, the variable range hopping [6,7,35] model, which describes the current associated with the hopping of electrons from one trap state to another distributed across different energies, is found to best represent the leakage evolution. The VRH mechanism, based on the theory developed by Mott and Hill, is illustrated in Figure 4b. The primary trap location is at A, with an energy E_T and an exponentially distributed density of states (DOS). Electrons can hop from A to empty trap positions situated at B or C, within a distance of R from the primary trap, and within a range of energy surrounding E_T .

The fit to measurements is presented in Figure 6 and modelled using the following relation with temperature T [7,35], valid for moderate to high electric fields, where F^2 represents the field contribution to strengthening the VRH conduction:

$$I_{VRH} = I_0 \exp \left[-1.76 \left(\frac{T_0}{T} \right)^{\frac{1}{4}} + C_{VRH} \left(\frac{T_0}{T} \right)^{\frac{3}{4}} F^2 \right], \quad (3)$$

I_0 modifies the trap emission rate into current, C_{VRH} represents a grouped constant, which can be written as $C_{VRH} = 4.626 \times 10^{-3} \times \left(\frac{qa}{U} \right)^2$ [7], where q is the elementary charge, while a and U are constants related to the physical properties of the trap states. U indicates the characteristic energy of the DOS, and a represents the localization radius of the wave function corresponding to the trapped electron. It can be estimated to the effective Bohr radius of the bound electron and lies within the range of 1 nm to 10 nm [7,27,30,36]. T_0 , the characteristic temperature, can be written as $T_0 = \frac{18}{(k_B D_T a^3)}$ [7,35,37,38]. It is inversely proportional to the trap DOS D_T (volume⁻¹ energy⁻¹) at the primary (see A in Figure 4b) trap energy and can vary depending on a . A summary of different T_0 values reported in the literature [7,24,25,27–30,33,37,39] is provided in Figure 7 for reference, showing consistent results for the values extrapolated in this paper.

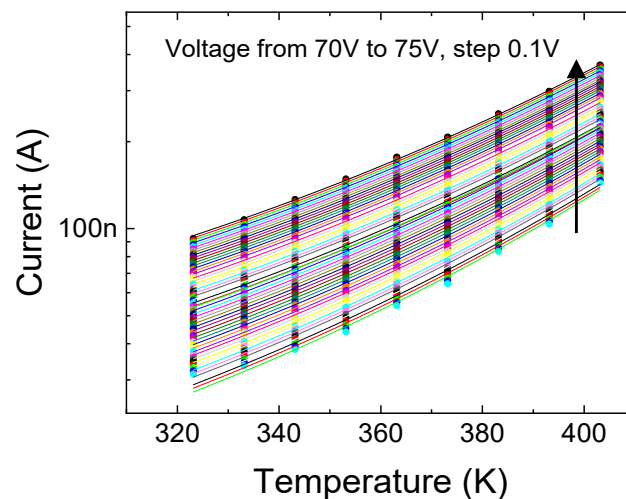


Figure 6. Modeling reverse leakage diode behavior using variable range hopping (VRH) from $V = -70$ V to -75 V (Region 2) for $T = 50$ °C (323 K) to 130 °C (403 K).

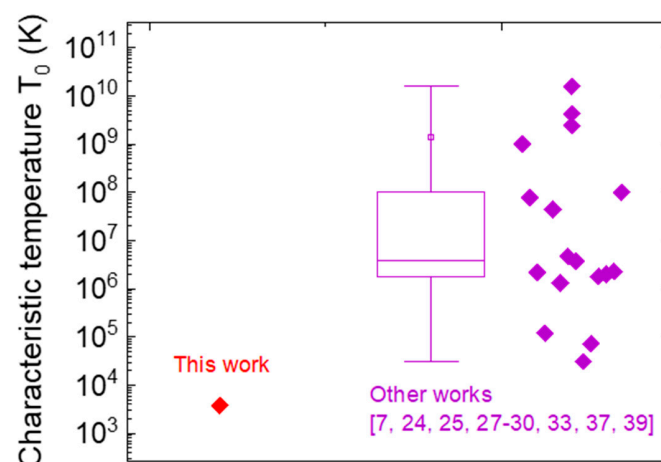


Figure 7. Comparison of the characteristic temperature (T_0) obtained from different works on GaN-based systems [7,24,25,27–30,33,37,39].

Based on these results, we conclude that a substantial reduction in leakage current and in its temperature sensitivity can be obtained through the reduction of the density of defects within the drift region. Specific attention needs to be focused on the residual carbon concentration, considering its contribution to the low voltage regime.

3.2. TCAD Simulations of Diode Breakdown

To obtain an estimate of the breakdown voltage of the test structures, several samples were subjected to reverse bias sweeps until failure at room temperature, as illustrated in Figure 8. Very little dispersion was observed within the diode characteristics, and the mean reverse breakdown voltage was found to be around 170 V (inset of Figure 8).

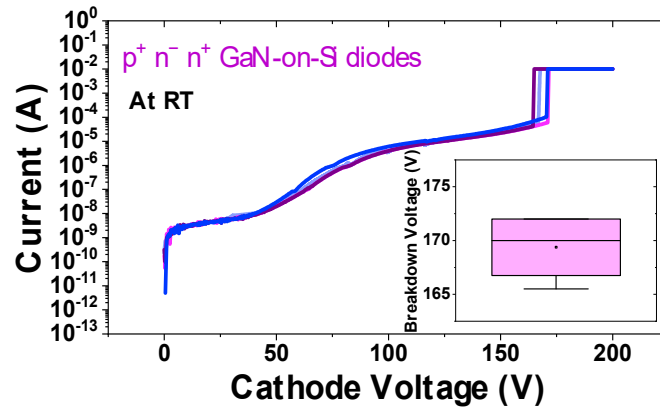


Figure 8. Reverse bias I–V diode characteristics until failure on four diodes. (inset) Mean breakdown voltage is 170 V.

The 2D-TCAD simulations, based on the drift–diffusion model for carrier transport, were employed to build a representative model of the measured devices, using the Sentaurus tool from Synopsys [40]. To investigate the nature of breakdown, a simplified fully vertical ($n^+p^+n^-n^+$) diode structure (see Figure 9a) was used. The anode and cathode are defined as modified ohmic contacts to improve accuracy around the p–n junction; it does not impose the charge neutrality condition at vertices within the charged depletion regions [40]. In addition to suitable mobility and recombination models, the gate-dependent strain polarization model, especially suited to GaN devices, was activated. Since Mg has a relatively high ionization energy of 0.16 eV [41,42], Mg acceptors are not completely ionized at room temperature. Thus, to correctly model the p-doping levels and reproduce the breakdown voltage, the incomplete ionization model in Sentaurus was used, which is physically more accurate to model Mg doping. The effective doping concentration was computed internally based on ionization probability, derived from the ionization energy of the doping species.

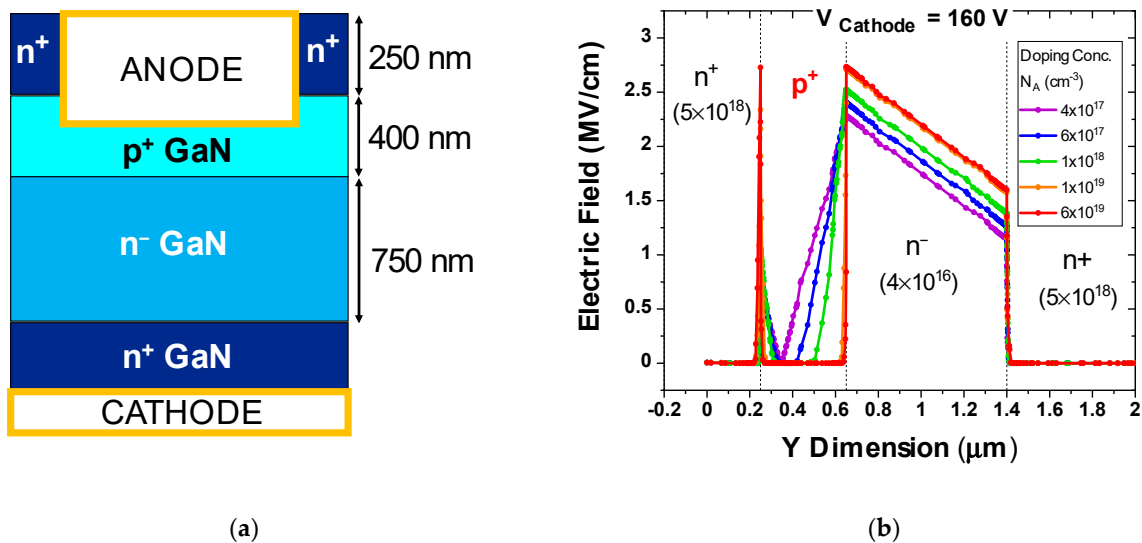


Figure 9. (a) Schematic of the simulated structure. (b) Electric field profile along the simulated vertical p^+n^- diode for $N_A = 4 \times 10^{17} \text{ cm}^{-3}$, $6 \times 10^{17} \text{ cm}^{-3}$, $1 \times 10^{18} \text{ cm}^{-3}$, $1 \times 10^{19} \text{ cm}^{-3}$, and $6 \times 10^{19} \text{ cm}^{-3}$.

Figure 9b presents the electric field evolution along the simulated structure as a function of the chosen p-doping level, for a cathode voltage of 160 V, i.e., just below the measured breakdown voltage.

For high p-doping, such as for $N_A = 6 \times 10^{19} \text{ cm}^{-3}$ (see Figure 10b), we observed the peak electric field at the p^+ to n^- interface approaching the critical field value for GaN (3.3 MV/cm [43]). The applied potential dropped almost entirely across the n-drift region, with little to negligible depletion observed within the p-GaN layer. As such, we can expect breakdown to occur when the peak electric field crosses E_{Crit} .

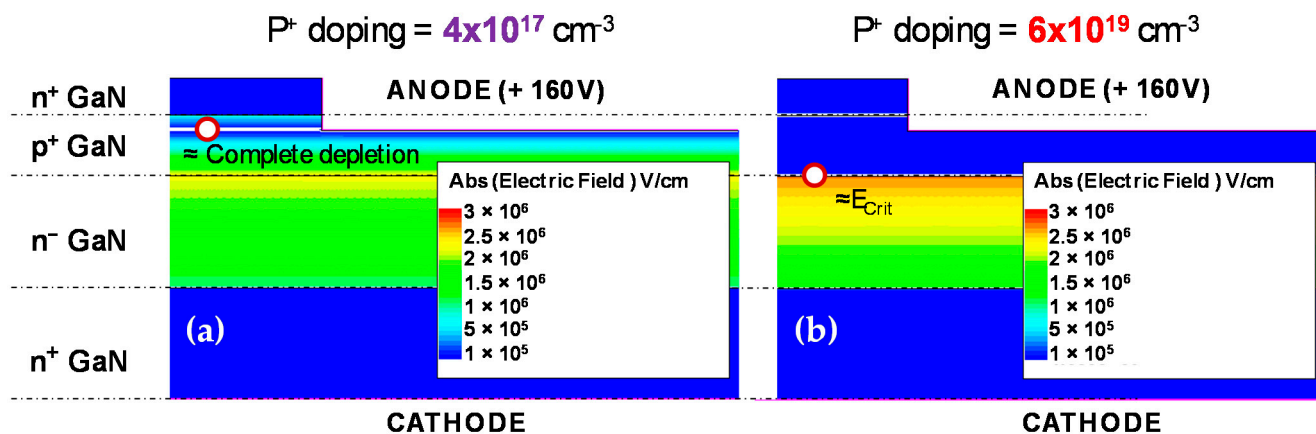


Figure 10. Two failure processes are identified from electric field profiles: (a) For lowly doped samples, punch-through occurs, due to the full depletion of the p-GaN, and (b) for high p-GaN, doping breakdown corresponds to the voltage for which the peak E-field at the p^+n junction reaches the critical field of GaN.

For the devices under test, the p-doping level was $N_A = 6 \times 10^{19} \text{ cm}^{-3}$, which indicates breakdown triggered by peak electric fields >3 MV/cm at the p^+n junction, as can be seen from the evolution of the electric field with increasing voltage in Figure 11.

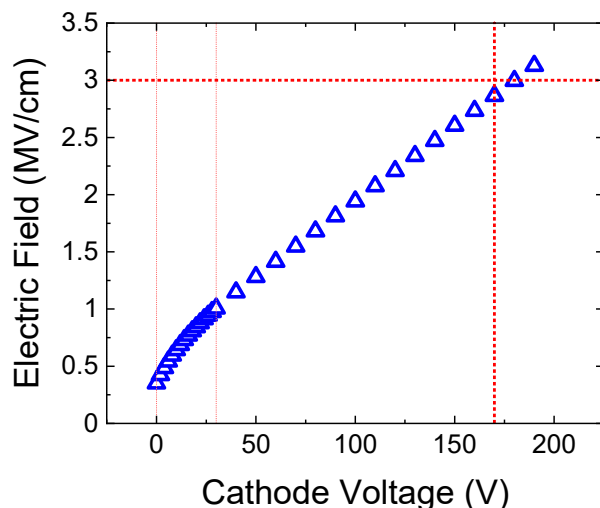


Figure 11. Electric field profile versus voltage for $N_A = 6 \times 10^{19} \text{ cm}^{-3}$, corresponding to the devices under test, illustrating a field value $\approx 3 \text{ MV/cm}$ at 170 V.

The field values obtained in the range of 0 V–30 V were used in Figure 3b to verify the $\Delta E_A \propto \sqrt{F}$ dependence. It can be expected that by decreasing the p-doping within a certain range, we can reduce the peak electric field (see Figure 10b for $N_A = 1 \times 10^{18} \text{ cm}^{-3}$), pushing V_{BR} to higher voltages >200 V. Simulations indicated that reducing the p-doping significantly introduces a different constraint. For example, for $N_A = 6 \times 10^{17} \text{ cm}^{-3}$, we observed a much wider depletion of the p-GaN region. If the p-doping levels are too low ($N_A = 4 \times 10^{17} \text{ cm}^{-3}$ in Figures 9b and 10a), complete depletion of the pGaN layer can

occur, thus leading to punch-through even before the peak electric field reaches E_{Crit} . This effect may be further worsened under real conditions by the presence of hydrogen during the epi-growth process [44], which would reduce the effective concentration of Mg and accelerate the punch-through.

Figure 12 illustrates the evolution of electric field and ionized acceptor concentration with cathode voltage, for low ($N_A = 4 \times 10^{17} \text{ cm}^{-3}$) and high p-doping ($N_A = 6 \times 10^{19} \text{ cm}^{-3}$) cases.

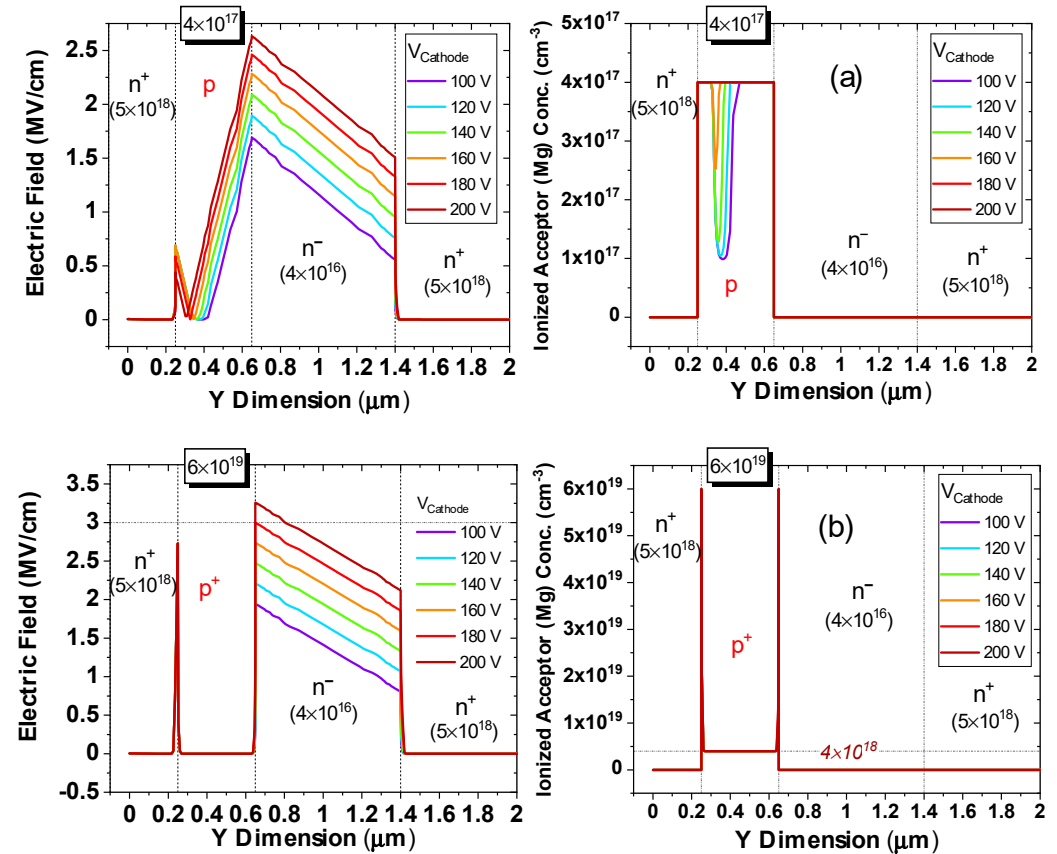


Figure 12. Electric field profile and ionized Mg acceptor concentration for simulations at different voltages with the incomplete ionization model: (a) low p-doping, $N_A = 4 \times 10^{17} \text{ cm}^{-3}$, (b) high p-doping, $N_A = 6 \times 10^{19} \text{ cm}^{-3}$. A trade-off exists on the value of p-doping: it must be sufficiently low to reduce the peak field, and sufficiently high to avoid punch-through.

First, from Figure 12b we note that the simulations accurately reproduced the breakdown voltage of 180 V, for the samples under analysis, that had a doping level equal to $N_A = 6 \times 10^{19} \text{ cm}^{-3}$. Second, we note that for the low N_A case (Figure 12a), the ionized Mg concentration followed the progressive depletion of the p-GaN layer with higher voltages, with complete ionization at voltages higher than the punch-through voltage.

Finally, for high N_A , the base ionization level was constant at 6% ($=4 \times 10^{18} \text{ cm}^{-3}$) of the defined N_A for most of the p^+ GaN layer, except at the pn junctions, where the Mg acceptors were almost fully ionized.

Our conclusion on this part is that a trade-off exists on the value of p-doping, which must be sufficiently low to reduce the peak field, and sufficiently high to avoid punch-through.

4. Conclusions

In summary, we presented a detailed analysis of the leakage and breakdown limits of semi-vertical GaN-on-Si test structures. The results of the analysis indicated that thermionic carrier emissions from a trap state of 0.85 eV dominates leakage at low voltage, while variable range hopping is observable at high voltage.

TCAD simulation of the p⁺n diodes is employed to reproduce the breakdown voltage of semi vertical GaN on Si diodes. For the measured test structures with $N_A = 6 \times 10^{19} \text{ cm}^{-3}$, breakdown is estimated to correspond to the voltage for which the peak E-field at the p⁺n junction reaches the critical field of GaN, and simulation can effectively reproduce the experimental results. For lowly doped samples, punch-through occurs, due to the full depletion of the p-GaN, as demonstrated by simulations. In conclusion, the doping of the p-GaN layer can strongly impact the breakdown voltage of the analyzed structures, and a trade-off between the occurrence of punch-through and junction breakdown needs to be considered to optimize device robustness.

Author Contributions: Conceptualization, K.M., C.D.S., M.B. (Matteo Buffolo), M.B. (Matteo Borga), A.G., S.Y., K.G., B.B., S.D., G.M., E.Z. and M.M.; investigation, K.M., C.D.S., M.B. (Matteo Buffolo), M.B. (Matteo Borga), S.Y., K.G., B.B., S.D., G.M., E.Z. and M.M.; data curation, K.M., C.D.S., B.B., S.Y. and M.M.; writing—original draft preparation, K.M., C.D.S., M.M., K.G., S.Y. and B.B.; writing—review and editing, K.M., C.D.S., M.M., K.G., S.Y. and B.B.; supervision, A.G., G.M., E.Z., M.M. and S.D.; funding acquisition, M.M. and S.D. All authors have read and agreed to the published version of the manuscript.

Funding: This project has received funding from the ECSEL Joint Undertaking (JU) under grant agreement No. 826392. The JU receives support from the European Union’s Horizon 2020 research and innovation program and Austria, Belgium, Germany, Italy, Norway, Slovakia, Spain, Sweden, and Switzerland. This research activity was partly funded by project “Novel vertical GaN-devices for next generation power conversion”, NoveGaN (University of Padova), through the STARS CoG Grants call. Part of this work was supported by MIUR (Italian Minister for Education) under the initiative “Departments of Excellence” (Law 232/2016).

Conflicts of Interest: The authors declare no conflict of interest.

References

1. Kizilyalli, I.C.; Edwards, A.P.; Nie, H.; Disney, D.; Bour, D. High Voltage Vertical GaN p-n Diodes with Avalanche Capability. *IEEE Trans. Electron Devices* **2013**, *60*, 3067–3070. [[CrossRef](#)]
2. Hu, J.; Zhang, Y.; Sun, M.; Piedra, D.; Chowdhury, N.; Palacios, T. Materials and processing issues in vertical GaN power electronics. *Mater. Sci. Semicond. Process.* **2018**, *78*, 75. [[CrossRef](#)]
3. Kizilyalli, I.C.; Edwards, A.P.; Nie, H.; Disney, D.; Bour, D. Review of the Recent Progress on GaN-Based Vertical Power Schottky Barrier Diodes (SBDs). *Electronics* **2019**, *8*, 575.
4. Zhang, Y.; Sun, M.; Piedra, D.; Azize, M.; Zhang, X.; Fujishima, T.; Palacios, T. GaN-on-Si Vertical Schottky and p-n Diodes. *IEEE Electron Device Lett.* **2014**, *35*, 618–620.
5. Zhang, Y.; Wong, H.Y.; Sun, M.; Joglekar, S.; Yu, L.; Braga, N.A.; Palacios, T. Design space and origin of off-state leakage in GaN vertical power diodes. In Proceedings of the 2015 IEEE International Electron Devices Meeting (IEDM), Washington, DC, USA, 7–9 December 2015.
6. Rackauskas, B.; Dalcanale, S.; Uren, M.J.; Kachi, T.; Kuball, M. Leakage mechanisms in GaN-on-GaN vertical pn diodes. *Appl. Phys. Lett.* **2018**, *112*, 233501. [[CrossRef](#)]
7. Musolino, M.; Van Treeck, D.; Tahraoui, A.; Scarparo, L.; De Santi, C.; Meneghini, M.; Riechert, H. A physical model for the reverse leakage current in (In,Ga)N/GaN light-emitting diodes based on nanowires. *J. Appl. Phys.* **2016**, *119*, 044502. [[CrossRef](#)]
8. Liu, C.; Khadar, R.A.; Matioli, E. GaN-on-Si Quasi-Vertical Power MOSFETs. *IEEE Electron Device Lett.* **2017**, *39*, 71–74. [[CrossRef](#)]
9. Otake, H.; Chikamatsu, K.; Yamaguchi, A.; Fujishima, T.; Ohta, H. Vertical GaN-Based Trench Gate Metal Oxide Semiconductor Field-Effect Transistors on GaN Bulk Substrates. *Appl. Phys. Express* **2018**, *1*, 011105. [[CrossRef](#)]
10. Mukherjee, K.; Borga, M.; Ruzzarin, M.; De Santi, C.; Stoffels, S.; You, S.; Meneghini, M. Analysis of threshold voltage instabilities in semi-vertical GaN-on-Si FETs. *Appl. Phys. Express* **2020**, *13*, 024004. [[CrossRef](#)]
11. Saremi, M. Modeling and Simulation of the Programmable Metallization Cells (PMCs) and Diamond-Based Power Devices. Ph.D. Thesis, Arizona State University, Tempe, AZ, USA, 2017.
12. Saremi, M.; Hathwar, R.; Dutta, M.; Koeck, F.A.; Nemanich, R.J.; Chowdhury, S.; Goodnick, S.M. Analysis of the reverse I-V characteristics of diamond-based PIN diodes. *Appl. Phys. Lett.* **2017**, *111*, 043507. [[CrossRef](#)]
13. Mahabadi, S.E.J.; Moghadam, H.A. Comprehensive study of a 4H-SiC MES-MOSFET. *Phys. E* **2015**, *74*, 5–29. [[CrossRef](#)]
14. Moghadam, H.A.; Dimitrijević, S.; Han, J.; Haasmann, D.; Aminbeidokhti, A. Transient-current method for measurement of active near-interface oxide traps in 4H-SiC MOS capacitors and MOSFETs. *IEEE Trans. Electron Devices* **2015**, *62*, 2670–2674. [[CrossRef](#)]
15. Liu, Z.; Li, P.G.; Zhi, Y.S.; Wang, X.L.; Chu, X.L.; Tang, W.H. Review of gallium oxide based field-effect transistors and Schottky barrier diodes. *Chin. Phys. B* **2019**, *28*, 017105. [[CrossRef](#)]
16. Palacios, T.A.; Fujishima, T. Aluminum Nitride Based Semiconductor Devices. U.S. Patent 9337301B2, 10 May 2016.

17. Han, D.P.; Oh, C.H.; Kim, H.; Shim, J.I.; Kim, K.S.; Shin, D.S. Conduction Mechanisms of Leakage Currents in InGaN/GaN-Based Light-Emitting Diodes. *IEEE Trans. Electron Devices* **2015**, *62*, 587–592.
18. Chiu, F.-C. A Review on Conduction Mechanisms in Dielectric Films. *Adv. Mater. Sci. Eng.* **2014**, *2014*, 1–18. [[CrossRef](#)]
19. Mazzola, M.S.; Sadow, S.E.; Neudeck, P.G.; Lakdawala, V.K.; We, S. Observation of the D-center in 6H-SiC p-n diodes grown by chemical vapor deposition. *Appl. Phys. Lett.* **1994**, *64*, 2730. [[CrossRef](#)]
20. Demchenko, D.O.; Diallo, I.C.; Reshchikov, M.A. Yellow Luminescence of Gallium Nitride Generated by Carbon Defect Complexes. *Phys. Rev. Lett.* **2013**, *110*, 087404. [[CrossRef](#)]
21. Huber, M.; Silvestri, M.; Knuutila, L.; Pozzovivo, G.; Andreev, A.; Kadashchuk, A.; Lundskog, A. Impact of residual carbon impurities and gallium vacancies on trapping effects in AlGaIn/GaN metal insulator semiconductor high electron mobility transistors. *Appl. Phys. Lett.* **2015**, *107*, 032106. [[CrossRef](#)]
22. Hill, R.M. Poole Frenkel conduction in amorphous solids. *Philos. Mag.* **1971**, *23*, 59. [[CrossRef](#)]
23. Frenkel, J. On Pre-Breakdown Phenomena in Insulators and Electronic Semi-Conductors. *Phys. Rev.* **1938**, *54*, 647. [[CrossRef](#)]
24. Shan, Q.; Meyaard, D.S.; Dai, Q.; Cho, J.; Fred Schubert, E.; Kon Son, J.; Sone, C. Transport-mechanism analysis of the reverse leakage current in GaInN light-emitting diodes. *Appl. Phys. Lett.* **2011**, *99*, 253506. [[CrossRef](#)]
25. Zhou, S.; Lv, J.; Yini, W.; Zhang, Y.; Zheng, C.; Liu, S. Reverse leakage current characteristics of InGaIn/GaN multiple quantum well ultraviolet/blue/green light-emitting diodes. *Jpn. J. Appl. Phys.* **2018**, *57*, 051003. [[CrossRef](#)]
26. Simmons, J.G. Conduction in thin dielectric films. *J. Phys. D Appl. Phys.* **1971**, *4*, 613. [[CrossRef](#)]
27. Kuksenkov, D.; Temkin, H.; Osinsky, A.; Gaska, R.; Khan, M. Origin of conductivity and low-frequency noise in reverse-biased GaN pn junction. *Appl. Phys. Lett.* **1998**, *72*, 1365–1367. [[CrossRef](#)]
28. Kim, J.; Kim, J.Y.; Tak, Y.; Kim, J.; Hong, H.G.; Yang, M.; Chung, U.I. Investigation of reverse leakage characteristics of InGaIn/GaN light-emitting diodes on silicon. *IEEE Electron Device Lett.* **2012**, *33*, 1741–1743. [[CrossRef](#)]
29. Jung, E.; Lee, J.K.; Kim, M.S.; Kim, H. Leakage Current Analysis of GaN-Based Light-Emitting Diodes Using a Parasitic Diode Model. *IEEE Trans. Electron Devices* **2015**, *62*, 3322–3325. [[CrossRef](#)]
30. Look, D.C.; Reynolds, D.C.; Kim, W.; Aktas, Ö.; Botchkarev, A.; Salvador, A.; Morkoç, A. Deep-center hopping conduction in GaN. *J. Appl. Phys.* **1996**, *80*, 2960–2963. [[CrossRef](#)]
31. Lee, M.; Lee, H.U.; Song, K.M.; Kim, J. Significant improvement of reverse leakage current characteristics of Si-based homoepitaxial InGaIn/GaN blue light emitting diodes. *Sci. Rep.* **2019**, *9*, 970. [[CrossRef](#)]
32. Hirsch, L.; Barrière, A.S. Electrical characterization of InGaIn/GaN light emitting diodes grown by molecular beam epitaxy. *J. Appl. Phys.* **2003**, *94*, 5014. [[CrossRef](#)]
33. Ferdous, M.S.; Wang, X.; Fairchild, M.N.; Hersee, S.D. Effect of threading defects on InGaIn/GaNInGaIn/GaN multiple quantum well light emitting diodes. *Appl. Phys. Lett.* **2007**, *91*, 231107. [[CrossRef](#)]
34. Kim, J.; Kim, J.; Tak, Y.; Chae, S.; Kim, J.; Park, Y. Effect of V-Shaped Pit Size on the Reverse Leakage Current of InGaIn/GaN Light-Emitting Diodes. *IEEE Electron Device Lett.* **2013**, *34*, 1409–1411. [[CrossRef](#)]
35. Hill, R.M. Hopping conduction in amorphous solids. *Philos. Mag.* **1971**, *24*, 1307. [[CrossRef](#)]
36. Pollak, M.; Riess, I.J. A percolation treatment of high-field hopping transport. *Phys. C Solid State Phys.* **1976**, *9*, 2339. [[CrossRef](#)]
37. Zhao, L.; Chen, L.; Yu, G.; Yan, D.; Yang, G.; Gu, X.; Lu, H. Tunneling-Hopping Transport Model for Reverse Leakage Current in InGaIn/GaN Blue Light-Emitting Diodes. *IEEE Photonics Technol. Lett.* **2017**, *29*, 1447–1450. [[CrossRef](#)]
38. Yu, D.; Wang, C.; Wehrenberg, B.L.; Guyot-Sionnest, P. Variable Range Hopping Conduction in Semiconductor Nanocrystal Solids. *Phys. Rev. Lett.* **2004**, *92*, 216802. [[CrossRef](#)]
39. Tsou, C.; Ji, M.; Bakhtiarly-Noodeh, M.; Detchprohm, T.; Dupuis, R.D.; Shen, S. Temperature-Dependent Leakage Current Characteristics of Homojunction GaN p-i-n Rectifiers Using Ion-Implantation Isolation. *IEEE Trans. Electron Devices* **2019**, *66*, 4273–4278. [[CrossRef](#)]
40. *Sentaurus Device User Guide*; Synopsys: Mountain View, CA, USA, 2015.
41. Podor, B. Thermal ionization energy of Mg acceptors in GaN: Effects of doping level and compensation. *Int. Conf. Solid State Cryst.* **2000**, *4412*, 299–303.
42. Sabui, G.; Parbrook, P.J.; Arredondo-Arechavala, M.; Shen, Z.J. Modeling and simulation of bulk gallium nitride power semiconductor devices. *Aip Adv.* **2016**, *6*, 055006. [[CrossRef](#)]
43. Cheng, K.; Liang, H.; Van Hove, M.; Geens, K.; De Jaeger, B.; Srivastava, P.; Chung, H. AlGaIn/GaN/AlGaIn Double Heterostructures Grown on 200 mm Silicon (111) Substrates with High Electron Mobility. *Appl. Phys. Express* **2012**, *5*, 011002. [[CrossRef](#)]
44. Yang, J.; Zhao, D.; Jiang, D.; Chen, P.; Zhu, J.; Liu, Z.; Du, G.T. Influence of hydrogen impurities on p-type resistivity in Mg-doped GaN films. *J. Vac. Sci. Technol. A* **2015**, *33*, 021505. [[CrossRef](#)]